

Influence of electric fields on the smectic layer structure of ferroelectric and antiferroelectric liquid crystal devices

S. J. Watson, L. S. Matkin, L. J. Baylis, N. Bowring, and H. F. Gleeson*

Department of Physics and Astronomy, University of Manchester, Manchester M13 9PL, United Kingdom

M. Hird and J. Goodby

School of Chemistry, Hull University, Hull HU6 7RJ, United Kingdom

(Received 17 July 2001; published 11 February 2002)

The electric-field-induced structural rearrangement of smectic layers in the antiferroelectric and ferroelectric phases of three different materials is reported. The materials all have high optical tilt angles (around 30°), compared with the steric tilt angles deduced from layer spacing measurements (around 18°). The chevron angles observed in devices agree well with values found for the steric tilt angle across the tilted mesophase range. Electric fields were applied to liquid crystal devices while the smectic layer structures, in both the depth and in the plane of the device, were probed using small angle x-ray scattering. Two separate aspects of the influence of the field on the layer structure were studied. First, the organization of the smectic layers in the antiferroelectric phase is described before, during, and after the application of an electric field of sufficient magnitude to induce a chevron to bookshelf transition. Second, the evolution of the field-induced layer structure change has been investigated as the field was incrementally increased in both the antiferroelectric and ferroelectric phases. It was found that the chevron to bookshelf transition has a distinct threshold in the antiferroelectric phase, but shows low or zero threshold behavior in the ferroelectric phase for all the materials studied.

DOI: 10.1103/PhysRevE.65.031705

PACS number(s): 42.70.Df

INTRODUCTION

The first experimental evidence of antiferroelectric ordering in a liquid crystal [1] was published several years after the discovery of ferroelectricity in liquid crystals [2]. In both ferroelectric and antiferroelectric liquid crystals the molecules are arranged in layers with the director tilted with respect to the layer normal by a temperature-dependent tilt angle [3]. The ferroelectric chiral smectic-C (SmC^*) structure is synclitic, the tilt direction modified only by a macroscopic helix that has a pitch typically hundreds of times greater than the layer spacing of $\sim 30 \text{ \AA}$. The antiferroelectric (SmC_A^*) structure is anticlinic, the tilt direction alternating from one layer to the next. Incorporating ferroelectric and antiferroelectric liquid crystals into display devices is extremely attractive [4], but although excellent prototype liquid crystal devices containing both types of materials exist, their widespread commercial use has not yet been realized. This is due in part to the complex electro-optic properties of ferroelectric and antiferroelectric devices, a consequence of the constraints that the device geometry imposes on the smectic layer structure.

Cooling from the orthogonal smectic-A (SmA) phase into a tilted phase causes a reduction in the smectic layer spacing and the layers in a device frequently adopt a chevron structure [5] to accommodate this layer shrinkage. The chevron geometry can be transformed to a bookshelf geometry on application of a sufficiently high electric field [6,7], a transi-

tion that usually occurs at a well-defined, high-field threshold ($\sim 5 \text{ V}/\mu\text{m}$) in ferroelectric liquid crystal devices [8]. Field-induced layer deformations are not restricted to the high-field regime. Time resolved x-ray diffraction experiments recently demonstrated reversible layer motion on the microsecond time scale in ferroelectric devices even at fields well below the chevron to bookshelf transition threshold [9]. Clearly, in the study of ferroelectric and antiferroelectric liquid crystal devices, it is important to examine both the static layer structure and the way in which it is deformed by fields. There are very few reports of the temperature dependence of the tilt angle [10], chevron angle [11] or chevron to bookshelf transition [12,13] in materials exhibiting antiferroelectric, ferroelectric, and ferroelectric liquid crystal phases. A brief report of an x-ray study of the evolution of the field-induced chevron to bookshelf transition in a device exhibiting all three SmC^* subphases was published recently [14], the results implying that the transition behavior depends on the phase type. This paper presents a detailed study of the temperature dependence of the chevron structure and tilt angles in three materials exhibiting ferro-, ferri-, and antiferroelectric phases. The complementary techniques of x-ray diffraction and electro-optic studies are employed to examine field-induced phenomena in the ferroelectric and antiferroelectric phases.

EXPERIMENT

The materials used in this work were synthesized at Hull University, UK and have been studied extensively by several authors [15–17]. The molecular structures are shown in Fig. 1 together with the phase sequences determined via microscopy and electro-optic methods. In the case of compounds 1 and 2, the assignment of the intermediate (ferrielectric)

*Corresponding author.

Email address: Helen.Gleeson@man.ac.uk

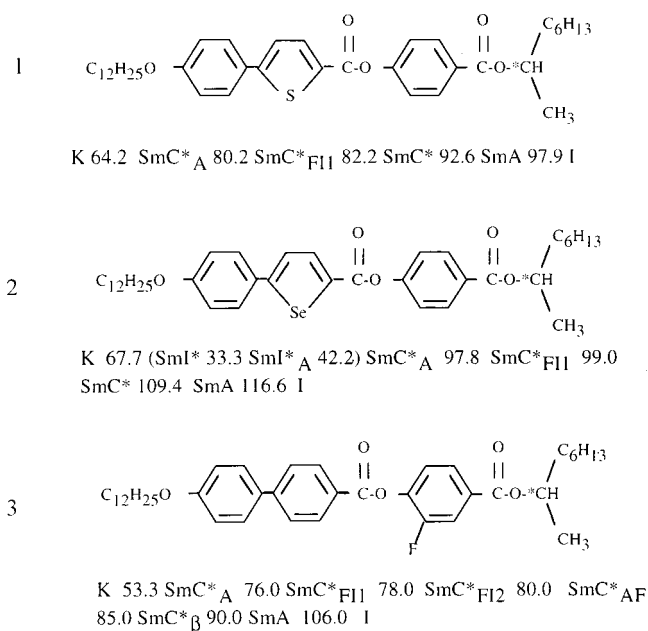


FIG. 1. The molecular structures and phase sequences of the three materials. SmI* and SmI*_A are hexatic ferroelectric and anti-ferroelectric phases, while SmC*_{F11} and SmC*_{F12} denote the three- and four-layer intermediate phases, respectively [20]. The phase sequence of compound 3 is as defined in Ref. [16], where SmC*_β and SmC*_{AF} are ferroelectric and intermediate phases respectively. K and I refer to the crystal and isotropic phases.

phases was also confirmed by resonant x-ray scattering [18–20]. The planar liquid crystal devices were constructed to a thickness of 15 μ m, as described elsewhere [14]. The materials all have short helical pitches and are not surface stabilized at this thickness. In all of the measurement techniques described below, the temperature of the devices was maintained with an absolute accuracy of ± 1 °C and a relative accuracy of ± 0.1 °C by use of a heating stage.

Optical tilt angle was measured with an accuracy of $\pm 0.5^\circ$ as described previously [10]. Spontaneous polarization (P_s) measurements were made using the current pulse technique [21] and were accurate to ± 2 nC/cm². The layer geometry of the devices was investigated using small angle x-ray diffraction at Daresbury SRS, UK as described elsewhere [14]. The smectic layer spacing of the three compounds was determined with an accuracy of ± 0.2 Å and used to determine the steric tilt angle ψ using the formula $\cos \psi = d/l$, where d is the smectic layer spacing and l is the molecular length [22].

X-ray rocking curves were obtained at specific temperatures in the liquid crystal samples by rocking the sample in 1° intervals over the range $\theta = -30^\circ - 30^\circ$ relative to the position where the plane of the cell is normal to the incident x-ray beam (Fig. 2). The intensity of the Bragg peak at each rocking position was integrated to produce rocking curves and the data were normalized to take account of the angular dependence of the glass absorption. Rocking curves provide information on the range and relative proportions of layer tilts in the device studied. In the geometry used, a bookshelf structure produces an intense peak around $\theta = 0^\circ$, whereas a

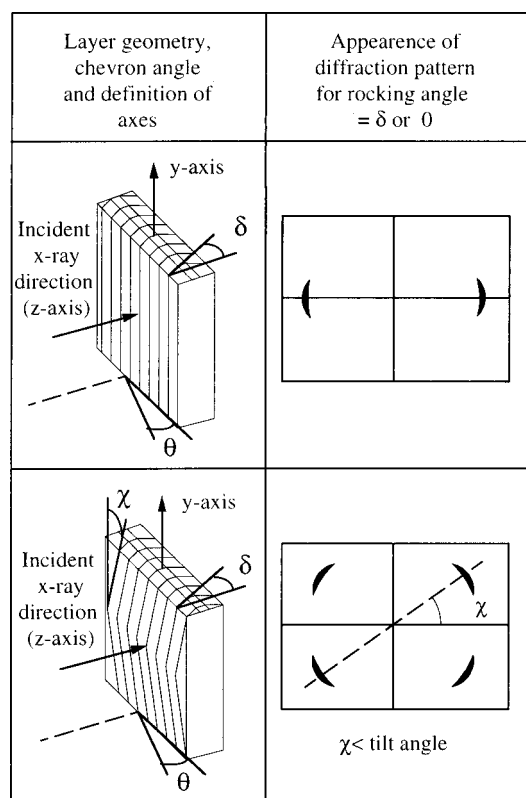


FIG. 2. The x-ray experimental geometry.

chevron structure shows intense peaks at the chevron angle. The chevron angle of the devices was determined as a function of temperature from the rocking curves to an accuracy of $\pm 0.5^\circ$. The use of an area detector allowed the layer orientation in the plane of the device to be studied (Fig. 2). A monodomain structure in which the smectic layer normal is perpendicular to both the incident x-ray beam direction and the rocking axis will produce a single set of peaks on the equator of the detector. Spreading or splitting of these peaks by an angle 2χ , indicates a distribution of the smectic layers in the plane of the device or an in-plane chevron respectively.

RESULTS AND DISCUSSION

Basic material properties

Layer spacing measurements of the three materials were obtained via x-ray diffraction, and the trends seen were similar to those reported previously in similar materials [10]. The spacing data were used to obtain steric tilt angles and Fig. 3 shows the temperature dependence of the chevron angle, the steric tilt angle, and the optical tilt angle of the materials. It can be seen from the figure that the chevron angle compares extremely well with measurements of the steric tilt angle at all temperatures. The optical tilt angles are all high, typically around 30° and are generally far greater than the steric tilt angle, indicating that the optically anisotropic molecular cores are significantly more tilted within the smectic layers than the terminal alkyl chains. The data for compound 3 show a marked crossover from a region where the steric tilt angle is greater than the optical tilt angle, to a region where

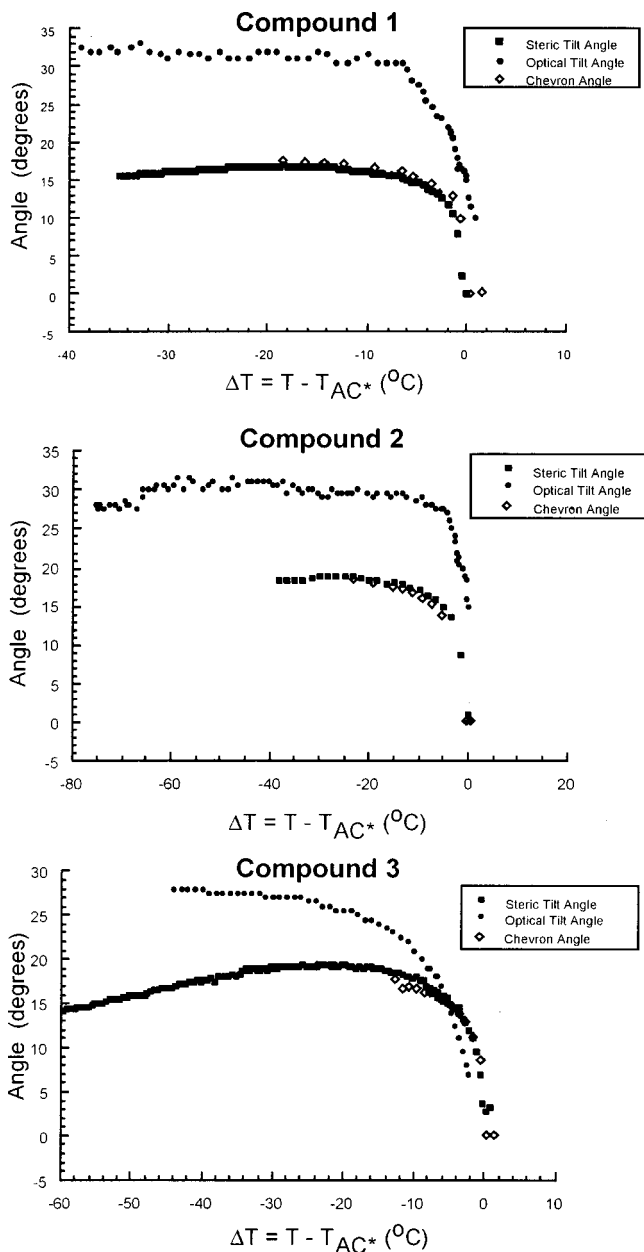


FIG. 3. The temperature dependence of the chevron, optical, and steric tilt angles for all three materials.

the reverse is true, a result that can be explained in terms of changing populations of conformers in the system [16]. The data of Fig. 3 illustrate a quite different correlation between the chevron angle and optical tilt angle than is normally observed for ferroelectric liquid crystal devices. Usually, the chevron angle is approximately 0.85 times the value of the optical tilt angle [3], while here the ratio is between 0.5 and 0.6.

The spontaneous polarization of the materials is relevant to a discussion of the electric-field effects. Figure 4 shows the variation of the saturated spontaneous polarization (P_s) as a function of temperature from the SmA to SmC* transition. It can be seen that the P_s is very similar for materials 1 and 2, taking a value of ~ 125 nC/cm² 40 °C below the orthogonal to tilted phase transition, and adopting a slightly

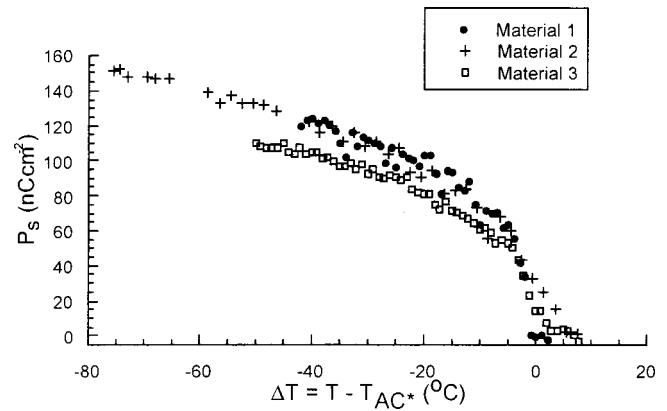


FIG. 4. The variation of spontaneous polarization with temperature for the three materials.

lower value (~ 105 nC/cm²) for material 3. These values of P_s are relatively large; for comparison, the commercially available ferroelectric material SCE 13 has a P_s of ~ 30 nC/cm². A large value of saturated spontaneous polarization is common in materials that exhibit antiferroelectric (AFE) and ferroelectric (FI) phases as large transverse dipoles are normally required for the formation of such phases.

The AFE layer structure before, during, and after applying large electric fields

There is evidence [19] that in some systems, fields that are sufficiently high to induce antiferroelectric to ferroelectric switching will also induce the chevron to bookshelf transition. Consequently, it is of interest to examine the layer structures adopted by antiferroelectric liquid crystals in devices before, during, and after the application of a switching field.

Temperatures were chosen within the antiferroelectric phase of each of the three samples and an electric field of 2.7 V/ μ m at 150 Hz (40-V square wave) was applied across the device. This voltage is sufficient to induce the chevron to bookshelf transition in each of the devices at the selected temperatures. Figure 5 shows the rocking curves obtained

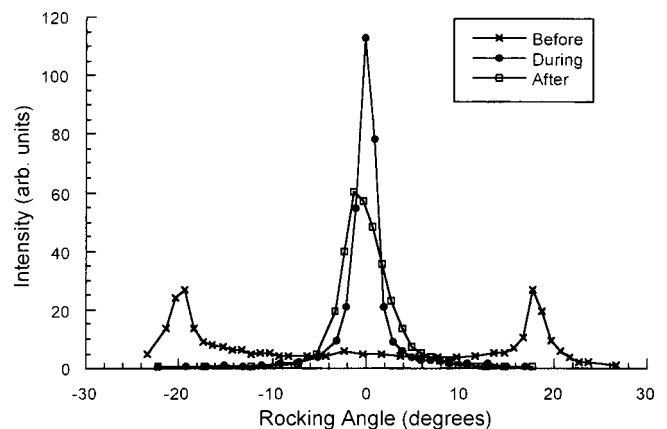


FIG. 5. Rocking curves acquired for compound 2 in the antiferroelectric phase before, during, and after the application of an electric field. This plot is typical of all the materials.

TABLE I. The full width at half maximum values (in degrees) for peaks in both θ and χ .

	Peak widths from rocking curves θ (rounded to the nearest 0.5°)			Peak widths from angular plots χ (rounded to the nearest 0.2°)		
	Before (at $\theta = \delta$)	During (at $\theta = 0^\circ$)	After (around $\theta = 0^\circ$)	Before (at $\theta = \delta$)	During (at $\theta = 0^\circ$)	After (at $\theta = 0^\circ$)
Material 1	1.0	1.0	4.5	3.2	4.8	5.2
Material 2	1.5	2.0	5.5	4.8	7.2	7.8
Material 3	1.5	3.0	10.5	9.6	42.0	36.6

before, during, and after the application of 40 V to a device containing compound 2 at a temperature of 90 °C. The rocking curves show that prior to the application of the field, the layers are arranged in a chevron geometry with a chevron angle of approximately 19°. The distribution of layers in θ is small; the peak at the chevron angle has a full width at half maximum (FWHM) of 1°. Application of the electric field causes the layers to rearrange to a bookshelf structure, producing an intense peak with a FWHM of 2° at a rocking angle of 0°. Upon removal of the field, the material adopts a deformed bookshelf structure, as indicated by the broad rocking curve (width of 5.5°) centered around 0° in Fig. 5. Similar data were obtained for devices containing compounds 1 and 3, though the rocking curves obtained following removal of the field do show some quantitative differences. The approximate full peak widths at half height before, during, and after field application are noted in Table I for all the materials studied. The widths of the relaxed layer structure in devices containing compounds 1 and 2 are both approximately 5°, though the distribution differs between the two devices with a significant retention of the sharp bookshelf feature in compound 1.

The rocking curves enable a distribution in θ to be determined, whilst an angular plot in χ about the origin gives information on the widths of the peaks resulting from a distribution in the plane of the device (Fig. 2). The area detector allows some measure of this effect and it is illustrative to consider the structural changes that can occur with applied field in the plane of the device. Table I shows the approximate full width at half height of the χ peaks at the chevron angle before field application and at $\theta = 0^\circ$ during and after field application.

The χ plots show a number of features that raise some interesting questions with regards to field-induced distortions of the in-plane smectic layer structure. These features are discussed in turn below.

Magnitude of the effect

The χ plots for all the materials show a clear broadening in the distribution of the in-plane layers upon field application. This is to be expected, as when the regular chevron structure is transformed into the bookshelf geometry, the in-plane layers must accommodate this by distorting or by the creation of a surface chevron. Upon removal of the field, the peak FWHM increases for materials 1 and 2, but decreases for material 3 (this decrease is discussed in more detail in the following section). In short, initially there is a well-defined

surface direction that distorts as the regular chevron to bookshelf transition takes place, as expected. After field application, the distribution in χ increases further for two of the devices, concurrent with an increase in the width of the peaks measured by the rocking curves. These data are consistent with a three-dimensional distortion and relaxation of the smectic layers occurring following the removal of the electric field.

Detail of the plots

Both materials 1 and 2 show only a broadening of the χ plots upon application of the electric field rather than a splitting or translation of the peaks, which would indicate a chevron or tilted bookshelf structure respectively. This broadening must be caused by a distribution of the smectic in-plane layers. Figure 6 shows the χ plot of material 3 upon application of electric field. A degree of splitting is clearly evident. Material 3 is the only compound that shows any evidence of a surface chevron being formed, and this splitting only occurs whilst the field is being applied. The in-plane chevron splitting is approximately 18°, the same as the regular chevron angle size at this temperature. It is also the only material that shows a decrease in the peak widths as the field is removed and this is most likely due to the relaxation of the in-plane chevron to a quasibookshelf structure.

Discussion of the θ and χ plots

Before field application, there exists a highly aligned chevron structure in all the materials. During field application, this is transformed to a well-aligned bookshelf geometry. It was initially thought that this transformation must be

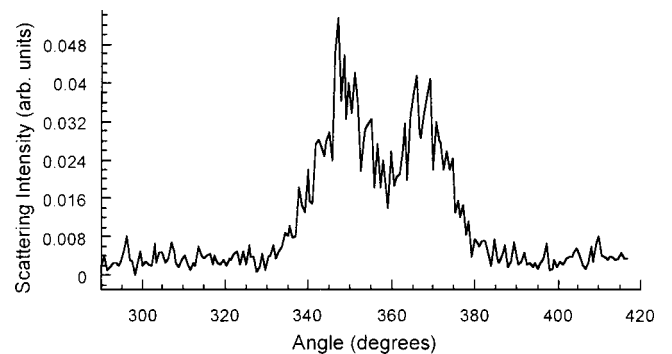


FIG. 6. The splitting in χ for material 3 seen during application of an electric field.

accompanied by the formation of a distinct surface chevron in the plane of the device. However, this phenomenon was observed in only one of the materials examined. At this time, the reasons for the differences in quantitative behavior between the materials are unknown, though several factors can be ruled out. There are no changes in the smectic layer spacing before, during, and after the application of a field, so the geometry changes are not being accommodated by a change in d . There is also no evidence of a tilted bookshelf being formed in the plane of the device, which would be noted by a shift in the χ position of the scattered peak. The proximity to the higher temperature ferroelectric phase is unlikely to be a factor in the quantitatively different behavior observed for each of the materials, as there are only a few degrees difference in reduced temperature between all the materials. The spontaneous polarization measurements are similar for all three compounds and all the applied voltages are well above the chevron to bookshelf threshold. Variations in layer elastic constants are a possible explanation, but there is no evidence to support this suggestion. Most importantly, other data suggest that the occurrence of split peaks is not even material or thickness dependent, nor is it phase dependent [23].

Although precautions were taken to standardize the cell-making procedure, fabrication differences between devices are inevitable, as, for example, the rubbing force and thickness of the alignment layer cannot be quantitatively recorded. It is clear from the peak width data that all the materials are not aligned to the same degree. Material 3 has larger peak widths in both θ and χ , and shows qualitative differences in field-off behavior. It may be that the field-induced structural changes are defined by the initial mosaicity of the device or by differences between devices in the surface anchoring energy. This is certainly an area of investigation that merits more work.

In summary, although it may be expected that the regular chevron to bookshelf transition must be accompanied by the formation of a surface chevron, it is clearly by no means the only way in which the geometric change can be accommodated. In fact, in the majority of cases studied, splitting of the peaks is not evident. In such cases, the geometric change must be accommodated by more subtle layer distortions or flow of the layers at the surfaces, as the phenomenon appears to be device dependent rather than material or thickness dependent.

Examination of the evolution of the field-induced layer structure in the AFE phase

We now consider the evolution of the field-induced layer deformation in the devices, in particular, pinpointing the threshold of the chevron to bookshelf transition. Temperatures were chosen within the antiferroelectric phase and ferroelectric phase of compounds 2 and 3 for this study. The devices were held at specific rocking angles and the intensity of the Bragg peak monitored as a function of the applied electric field. The applied voltage (150-Hz a.c. square wave form) was increased in 1 V steps and held at each incremental voltage for approximately 1 min whilst the x-ray scattering intensity was measured, so the experiment is quasistatic.

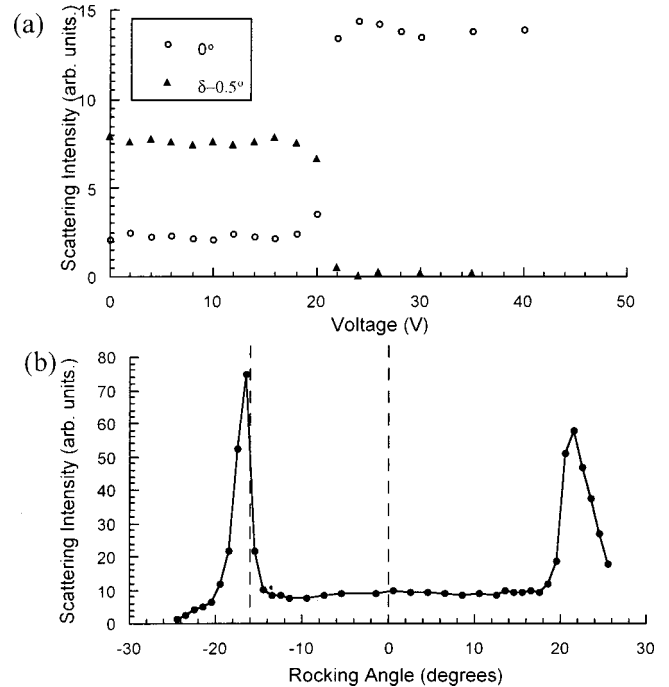


FIG. 7. (a) X-ray scattering intensity as a function of applied voltage for different angles θ and (b) the rocking curve with indication of angles at which the scattering intensity was examined in the antiferroelectric phase (70 °C) of compound 3.

Before each electric-field deformation experiment, the sample was heated to the untilted SmA phase and then cooled slowly to the required temperature, to produce identical structures prior to the application of the electric field. The field dependence of the Bragg peak intensity was measured at the bookshelf angle, the chevron angle, and several angles in between for each selected temperature. Thus, data were obtained that described the field dependence of the proportion of layers tilted at a specific angle with respect to the device substrates. Both materials 2 and 3 were examined in this way and the results are presented below. Although the results are qualitatively the same for both materials, the discussion of the results for material 3 is slightly more straightforward and for this reason will be considered first.

Figure 7(a) shows the field evolution of the intensity of the Bragg scattering peaks at selected rocking angles for material 3 in the antiferroelectric phase at 70 °C. Figure 7(b) shows the rocking curve before field application, and marked on it are the angles at which the layer motion was examined. It is clear that at 0 V, a large scattering intensity is measured just half a degree from the chevron angle $\delta = -0.5^\circ$ whilst there is practically no contribution at the bookshelf angle or at intermediate angles. The smectic layers are predominantly tilted at the chevron angle, as expected prior to the application of a field. A sharp transition is observed at ~ 20 V (1.3 V/ μm for this particular device) with a marked change in the Bragg peak intensity at the selected observation angles occurring over a 2 V range. At the transition, the scattering intensity from the layers at the chevron angle falls to zero, while the contribution from the bookshelf arrangement, with the device held at $\theta = 0^\circ$, increases concurrently. Data taken

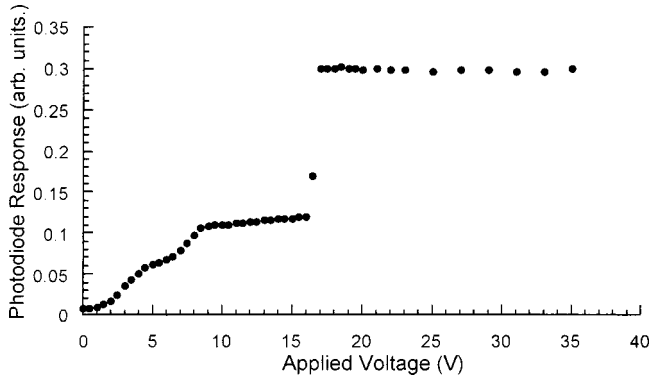


FIG. 8. Optical transmission data as a function of applied field, taken with a polarizing microscope and photodiode in the antiferroelectric phase of compound 3 (70 °C).

at intermediate rocking angles are not shown as effectively no scattering intensity was observed for such angles.

The optical transmission data obtained for compound 3 in the antiferroelectric phase are shown in Fig. 8 and two transitions are apparent. A thresholdless change in transmission is observed as the voltage is increased from 0 V that can be attributed to helical unwinding. At about 8 V (0.5 V/ μm in this device) it is clear from monitoring the switching behavior that ferroelectric switching commences. At around 17 V (1.1 V/ μm) there is a sharp threshold that is accompanied by a distinct change in texture. This final field-induced transition is in good agreement with the chevron to bookshelf transition confirmed by the x-ray data.

Figure 9 shows x-ray data corresponding to the field evolution of layer deformations for material 2 in the AFE phase at 80 °C and the rocking curve obtained prior to applying a field, with the angles under examination marked on it. The data in Fig. 9(a) show clearly the transition to the bookshelf structure, with a threshold of 2 V/ μm (30 V for this 15- μm thick device). The data indicate that the chevron to bookshelf transition is not as sharp as that in compound 3, occurring over a 3 V range and there appears to be a very small contribution from intermediate angles at the point of the transition. This may indicate a certain amount of disruption of the layers or a small amount of layer bend, or may be just due to defects in the texture. Most notably in this material, after the chevron to bookshelf transition, the bookshelf scattering contribution does not level off as might be expected, and the chevron intensity at δ does not reduce to zero as rapidly as was observed in compound 1. At present, the reason for this remains unknown. The scattering intensity must level off at higher fields, but the voltages required to test this were prohibitively high, and may have resulted in damage to the device. There is some evidence to suggest that the alignment of the stable state, (be that chevron or bookshelf) improves not only with increased voltage but also with time [8,24]. Unfortunately, the optical transmission data (Fig. 10) could not be carried out on the same device as used during the x-ray work, so the voltage thresholds cannot be compared directly. Nonetheless, qualitatively, it is clear that the behavior of the optical transmission differs from that seen in Fig. 8 for compound 3. There is no change in transmission until a distinct

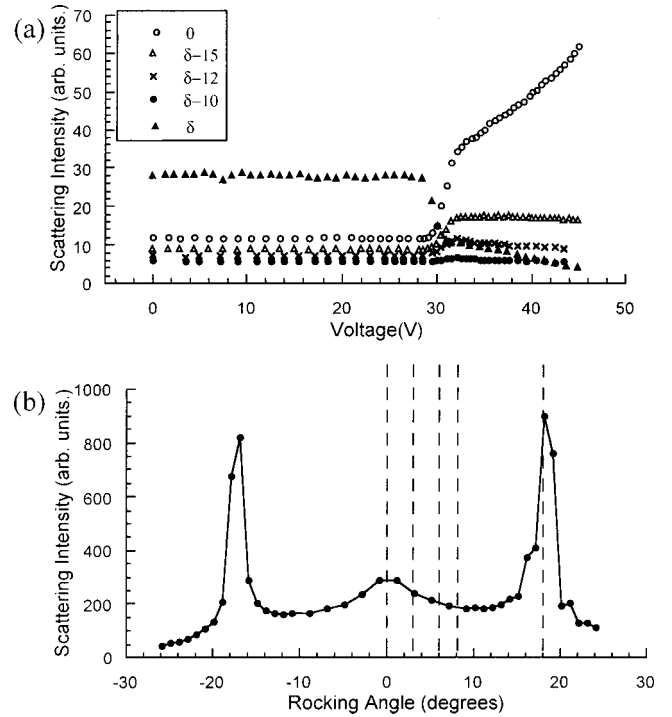


FIG. 9. (a) X-ray scattering intensity as a function of applied voltage for different angles of device orientation (θ) and (b) the rocking curve with indication of angles at which the scattering intensity was examined in the antiferroelectric phase (80 °C) of compound 2.

transition at 19 V. Combined with microscopic observations, this appears to indicate that the chevron to bookshelf transition is effectively coincident with the transition to ferroelectric switching. There is no evidence of helical unwinding, which is consistent with observations obtained via resonant scattering on this material [24].

Examination of the evolution of the field-induced layer structure in the FE phase

The SmC* devices and materials studied here show behavior very different from that reported previously for devices that employed low P_s , long pitch materials and

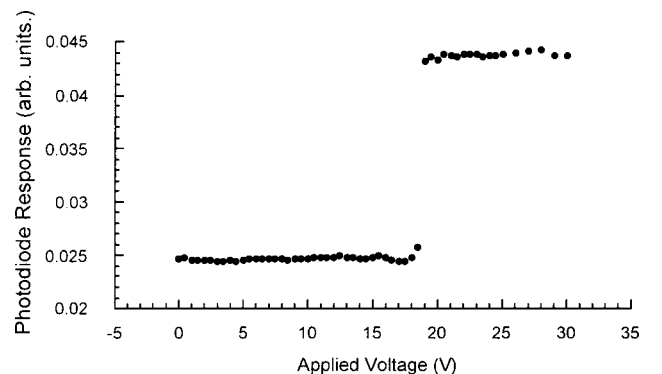


FIG. 10. Optical transmission data as a function of applied field, taken with a polarizing microscope and photodiode in the antiferroelectric phase of compound 2 (80 °C).

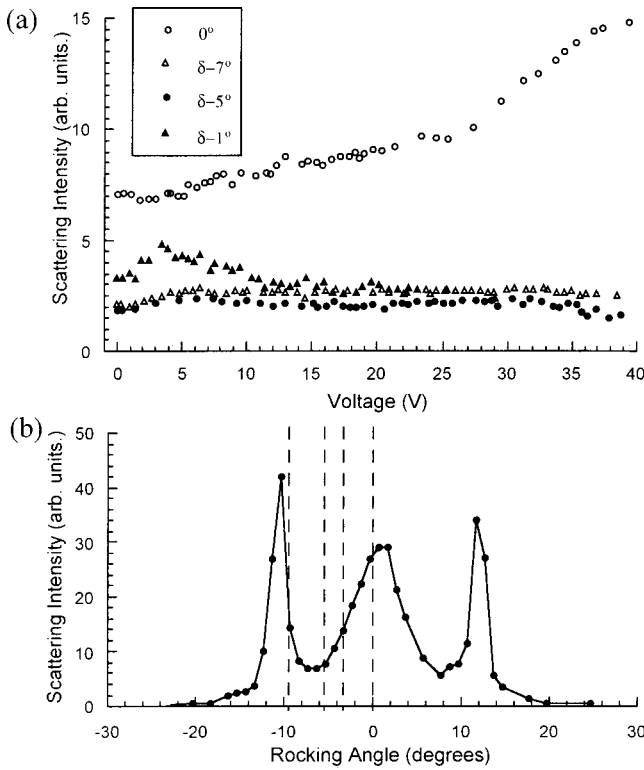


FIG. 11. (a) X-ray scattering intensity as a function of applied voltage for different angles of device orientation (θ) and (b) the rocking curve with indication of angles at which the scattering intensity was examined in the ferroelectric phase (92°C) of compound 3.

showed distinct, high-field thresholds for the chevron to bookshelf transition [8]. Figure 11(a) shows the field evolution for the ferroelectric phase of compound 3 at 92°C . The rocking curve obtained [Fig. 11(b)] shows a significant amount of bookshelf structure. The sharpness of the chevron peak meant that the scattering contribution at the bookshelf condition is greater, thus a higher intensity is seen in Fig. 11(a) for the bookshelf, $\theta=0^\circ$ condition than at $\theta=\delta^\circ-1^\circ$.

The field evolution data for the ferroelectric phase of compound 2 is shown in Fig. 12(a) and it is clear that the data are very similar to that of compound 3. The layer deformations in this phase are markedly different from those seen in the AFE phase. The scattering intensity data from the device held at 0° indicates that as the applied voltage is increased, the proportion of layers in the bookshelf geometry gradually increases with no distinct threshold, whilst the scattering contribution from layers in the chevron structure reduces. There was no significant scattering at intermediate angles, though the layers appear to move through angles slightly smaller than the chevron angle at low voltages. It is suggested that a possible structural evolution for this phase involves the proportion of bookshelf layers gradually growing at the expense of the chevron geometry, with no intermediate layer bending. The optical transmission data for both materials (not shown) appear to be consistent with the x-ray results, showing thresholdless behavior. The field evolution of a laterally fluorinated equivalent of compound 2 was also

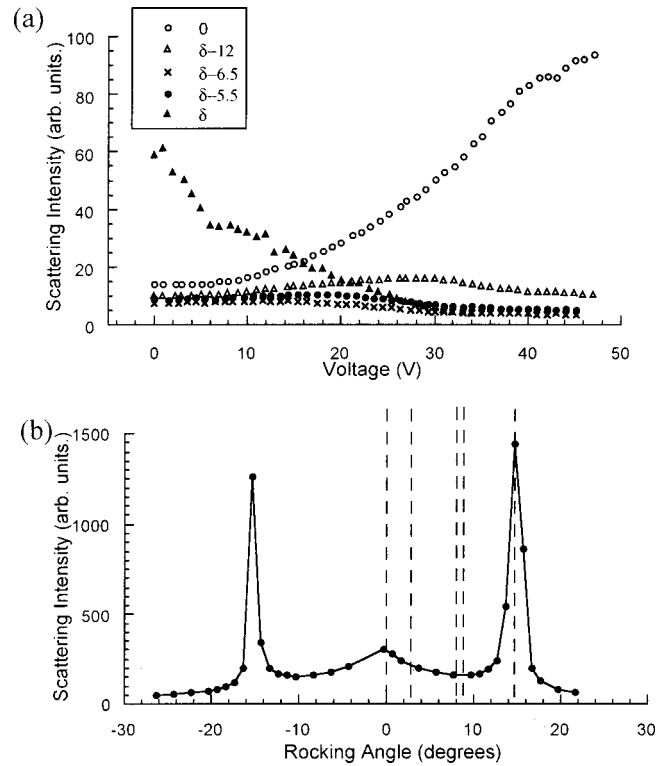


FIG. 12. (a) X-ray scattering intensity as a function of applied voltage for different angles θ and (b) the rocking curve with indication of angles at which the scattering intensity was examined in the ferroelectric phase (107°C) of compound 2.

examined in the FE phase, with similar “thresholdless” layer motion as for compounds 2 and 3. We conclude that the chevron to bookshelf transition for all of these materials is in marked contrast to previously reported chevron to bookshelf transitions in ferroelectric devices [3] that show distinct, high-field thresholds.

CONCLUSIONS

This paper presents an examination of some of the electro-optic characteristics of three different materials showing antiferro-, ferri-, and ferroelectric phase behavior. The optical tilt angles of all the materials are relatively high, and the steric and chevron angles correspond well with each other. The spontaneous polarization measurements are large, as is usual in materials with AFE and ferroelectric subphases.

A static x-ray study was carried out to examine the rearrangement of smectic layers within the antiferroelectric phase of the materials. It was found that upon removal of the field, the field-induced bookshelf geometry persisted, although the extent to which the alignment was retained differed amongst the three materials. The structural arrangement of the in-plane smectic layers was also considered and it was found that the destruction of the regular chevron did not necessarily result in the formation of a surface chevron or a tilted bookshelf geometry. However, when this did occur, the chevron angle was the same as that seen for the regular chevron before field application. The reason for the differences in behavior between the devices is not material or

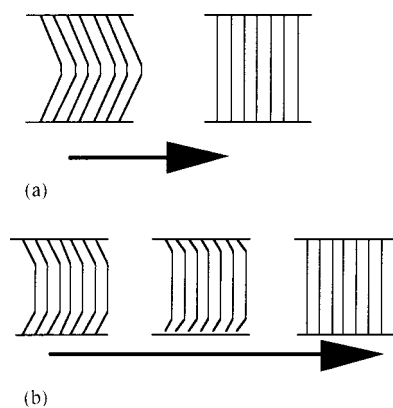


FIG. 13. Proposed models for layer motion upon application of electric fields in (a) the antiferroelectric phase and (b) the ferroelectric phase. The arrow indicates the direction of increasing field.

thickness dependent, and is most likely due to differences in surface anchoring strength, accommodating layer flow in some devices, but not others.

Figure 13 shows possible models for the layer motion in the depth of the device in both the antiferroelectric phase and the ferroelectric phase. In the antiferroelectric phase of all the materials studied, a distinct transition from the chevron to bookshelf geometry is observed, with no evidence of any intermediate layer bend or distortion. In the ferroelectric phase, the chevron to bookshelf transition is not distinct, occurring without a threshold. The amount of bookshelf ordering in the FE phase increases gradually with field as can be seen from the continuous increase in the intensity of the

Bragg peak at 0° , at the expense of the decreasing proportion of layers at the chevron angle. There is little scattering from intermediate angles, indicating that there is no curved intermediate structure, as seen in a previous study in the ferroelectric phase [14]. The small increase in the Bragg intensity with the device held just below the chevron angle, provides some evidence that the growth of the bookshelf geometry causes a slight distortion of the chevron angle. The difference between the field-induced layer deformations in the two phases cannot be related to the threshold for ferroelectric switching in the SmC_A^* phase (optical transmission data show this can occur below or coincident with the chevron to bookshelf transition). The differences can also not be attributed to saturated P_s values that change little over the temperature range studied. The threshold differences must, therefore, be due to variations in the layer elastic constants or in molecular arrangement between phases. These results demonstrate that in the ferroelectric phase, the assumption that there is no layer motion at low applied fields is clearly invalid. We believe that this observation is of importance in interpreting any electric-field related measurements (e.g., electro-optic, dielectric, etc.) undertaken on the SmC^* phases of this type of material.

ACKNOWLEDGMENTS

The financial support of the Engineering and Physical Sciences Research Council and Lucent Technologies (L.S.M.) is gratefully acknowledged. Thanks are also due to the staff of station 2.1 at the SRS, Daresbury, where the x-ray studies were carried out.

-
- [1] L. A. Beresenev, L. M. Blinov, V. A. Baikalov, E. P. Pozhdayev, G. V. Purvanetskias, and A. I. Pavluchenko, *Mol. Cryst. Liq. Cryst.* **89**, 327 (1982).
- [2] R. B. Meyer, L. Liebert, L. Strzelecki, P. Keller, *J. Phys. (France) Lett.* **36**, L69 (1975).
- [3] J. W. Goodby *et al.*, *Ferroelectric Liquid Crystals, Principles, Properties and Applications* (Gordon and Breach, Philadelphia, 1991).
- [4] S.T. Lagerwall *et al.*, *Ferroelectric and Antiferroelectric Liquid Crystals* (Wiley-VCH, Weinheim, 1999).
- [5] T. P. Reiker, N. A. Clark, G. S. Smith, D. S. Parmar, E. B. Sirota, and C. R. Safinya, *Phys. Rev. Lett.* **59**, 2658 (1987).
- [6] J. S. Patel, Sin-Doo Lee, and J. W. Goodby, *Phys. Rev. A* **40**, 2854 (1989).
- [7] G. Srajer, R. Pindak, and J. S. Patel, *Phys. Rev. A* **43**, 5744 (1990).
- [8] G. K. Bryant and H. F. Gleeson, *Ferroelectrics* **214**, 35 (1998), and references therein.
- [9] A. S. Morse, H. F. Gleeson, and S. Cummings, *Liq. Cryst.* **23**, 717 (1997); H. F. Gleeson, G. K. Bryant, and A. S. Morse, *Mol. Cryst. Liq. Cryst.* **362**, 203 (2001).
- [10] J. T. Mills, H. F. Gleeson, J. W. Goodby, M. Hird, A. Seed, and P. Styring, *J. Mater. Chem.* **8**, 2385 (1998).
- [11] P. Cluzeau, P. Barois, H. T. Nguyen, and C. Destrade, *Eur. Phys. J. B* **3**, 73 (1998).
- [12] M. Johnno, A. D. L. Chandani, Y. Ouchi, H. Takezoe, A. Fukuda, M. Ichihashi, and K. Furukawa, *Jpn. J. Appl. Phys., Part 2* **28**, L119 (1989); M. Johnno, Y. Ouchi, H. Takezoe, A. Fukuda, K. Trashima, and K. Furukawa, *ibid.* **29**, L111 (1990).
- [13] K. Itoh, M. Johnno, Y. Ouchi, H. Takezoe, and A. Fukuda, *Jpn. J. Appl. Phys., Part 1* **30**, 735 (1991).
- [14] L. S. Matkin, H. F. Gleeson, L. J. Baylis, S. J. Watson, N. Bowring, A. Seed, M. Hird, and J. W. Goodby, *Appl. Phys. Lett.* **77**, 340 (2000).
- [15] Y. Panarin, O. Kalinovskaya, and J. K. Vij, *Phys. Rev. E* **55**, 4345 (1997).
- [16] H. F. Gleeson, L. Baylis, W. K. Robinson, J. T. Mills, J. W. Goodby, A. Seed, M. Hird, P. Styring, C. Ronsenblatt, and S. Zhang, *Liq. Cryst.* **26**, 1415 (1999).
- [17] L. J. Baylis, H. F. Gleeson, A. J. Seed, P. J. Styring, M. Hird, and J. W. Goodby, *Mol. Cryst. Liq. Cryst.* **328**, 13 (1999).
- [18] P. Mach, R. Pindak, A. M. Levelut, P. Barois, H. T. Nguyen, C. C. Huang, and L. Furenlid, *Phys. Rev. E* **60**, 6793 (1999).

- [19] L. S. Matkin, H. F. Gleeson, P. Mach, C. C. Huang, R. Pindak, G. Srajer, J. Pollmann, J. W. Goodby, M. Hird, and A. J. Seed, *Appl. Phys. Lett.* **76**, 1863 (2000).
- [20] A. Cady, J. A. Pitney, R. Pindak, L. S. Matkin, S. J. Watson, H. F. Gleeson, P. Cluzeau, P. Barois, A.-M. Levelut, W. Caliebe, J. W. Goodby, M. Hird, and C. C. Huang. *Phys. Rev. E* **64**, 050702(R) (2001).
- [21] K. Miyasato, S. Abe, H. Takezoe, A. Fukuda, and E. Kuze, *Jpn. J. Appl. Phys., Part 2* **22**, L661 (1983).
- [22] J. T. Mills, R. Miller, H. F. Gleeson, A. J. Seed, M. Hird, and P. J. Styring, *Mol. Cryst. Liq. Cryst.* **303**, 145 (1997).
- [23] S. J. Watson, L. S. Matkin, and H. F. Gleeson (unpublished).
- [24] L. S. Matkin *et al.*, *Phys. Rev. E* **64**, 021705 (2001).